THE JOURNAL OF PHYSICAL CHEMISTRY C

ARTICLE

pubs.acs.org/JPCC

Tracing Gold Nanoparticle Charge by Electrolyte−Insulator−Semiconductor Devices

Jenny Gun,[*,†] Vitaly Gutkin,[†] Ovadia Lev,[†] Hans-Gerd Boyen,[‡] Marc Saitner,[‡] Patrick Wagner,[‡,§] Marc D'Olieslaeger,[‡,§] Maryam H. Abouzar,[⊥,∥] Arshak Poghossian,[⊥,∥] and Michael J. Schöning[*,⊥,∥]

[†]The Casali Institute and The Institute of Chemistry, The Hebrew University of Jerusalem, Givat Ram, Jerusalem, IL-91904, Israel

[‡]Institute for Materials Research (IMO), Hasselt University, B-3590 Diepenbeek, Belgium

[§]IMEC, division IMOMEC, 3590 Diepenbeek, Belgium

[⊥]Institute of Nano- and Biotechnologies (INB), Aachen University of Applied Sciences, Campus Jülich, Heinrich-Mußmann-Str. 1, DE-52428 Jülich, Germany

[∥]Institute of Bio- and Nanosystems (IBN-2), Research Centre Jülich, DE-52425 Jülich, Germany

ABSTRACT:

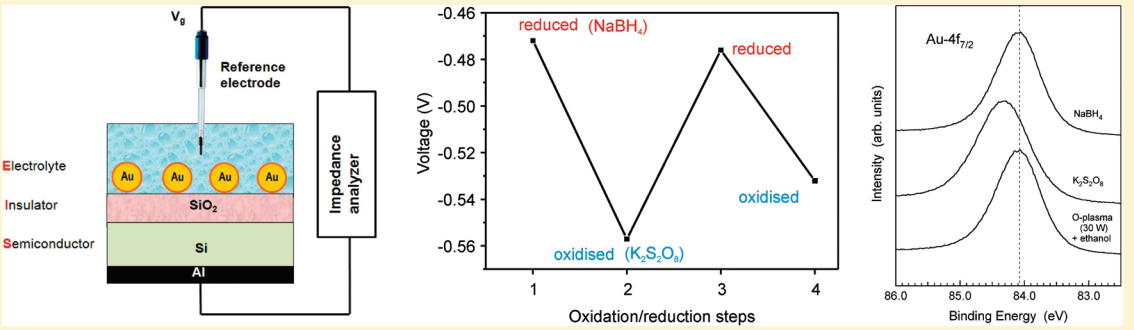

A capacitive field-effect electrolyte−insulator−semiconductor (EIS) device was applied for the first time to trace the charge of supported gold nanoparticles (Au-NPs) induced by oxygen plasma treatment or due to storing in aqueous oxidation and reduction solutions. In addition, X-ray photoelectron spectroscopy (XPS) has been used as a reference method to establish the various charge states of the Au-NPs resulting from the different treatment steps. After the oxygen-plasma treatment, a shift of the capacitance−voltage ($C-V$) curve (and flatband potential) of the Au-NP-covered p-Si−SiO_2 EIS structure by about −300 mV was found. The exposure of the EIS sensor surface to an oxidative and a reductive solution resulted in a shift of the $C-V$ curve for −85 and +81 mV, respectively. These observations correlate well with corresponding binding energy shifts in Au 4f core spectra in XPS experiments. The obtained results may open new opportunities for biosensing and biochips based on nanoparticle-charge-gated field-effect devices.

1. INTRODUCTION

Assemblies of bare and modified (with ligands containing different functional groups) gold nanoparticles (Au-NPs) on planar surfaces are an emerging and highly attractive class of electrically or chemically tunable functional materials with unique catalytic, optical, and electronic properties. Charging of Au-NPs in a controlled manner and storage and manipulation of charges is a vivid field of activity attracting not only fundamental research involving, for instance, adsorption and binding of molecules, bio- and photocatalysis, charge accumulation, and transport in nanoscaled materials (see, e.g., refs 1−3), but also application-oriented research ranging from (bio)chemical sensing and biochips[4−10] over molecular logic gates[11,12] and drug delivery systems[13] up to optical, electronic, and memory devices.[3,14,15] An electrochemical control over the Fermi level of a solid assembly of Au-NPs in contact with a macroscopic semiconductor transducer allows for the active tuning of electronic properties of the nanoparticle/transducer interface.[3] Generally, it is widely believed that a hybrid device approach involving the integration of nano-objects (e.g., NPs, nanotubes, biomolecules) with a macroscopic electronic transducer might be a more realistic approach for the transformation of their unique functional properties into macroscopically measurable effects.

The techniques used for the study of NP charging effects include discrete particle charging by scanning tunneling microscopy/spectroscopy (STM/STS),[16,17] electrochemical and, particularly, voltammetric studies,[18] surface plasmon resonance,[19,20] and X-ray photoelectron spectroscopy (XPS).[21−23] Scanning probe methods (STM/STS) generally require conductive supports combined with ultra-high-vacuum (UHV) conditions. The

Received: October 15, 2010
Revised: January 28, 2011
Published: February 24, 2011

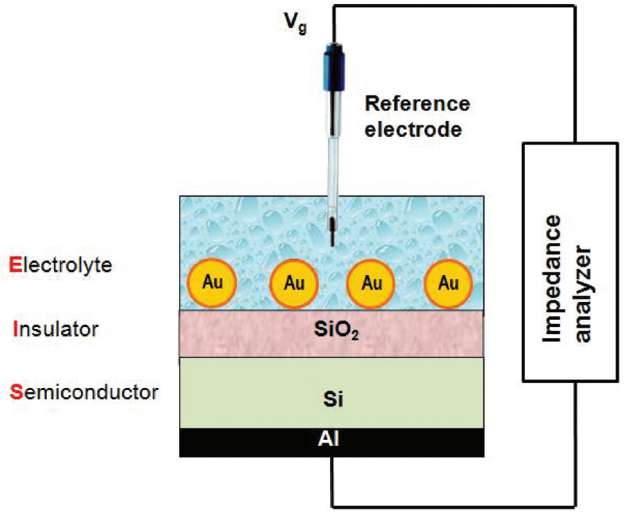

Figure 1. Schematic of the Au-NP-modified capacitive EIS structure.

electrochemical methods discussed in the literature also rely on the availability of conductive substrates and, in addition, on NP passivation layers to prevent a rapid dissipation of the accumulated charge from the NPs into their supports. The plasmon resonance technique does not require conductive support; however, it is insensitive to particle sizes below 2 nm and its sensitivity is insufficient for many potential fields of application.[24] The last method, XPS, is, in principle, the most direct one, because the Au 4f binding energy shift can provide quantitative information about the transfer of electrons from or to their supports. However, XPS needs conducting supports and UHV conditions as well, making it unsuitable for rapid online monitoring of, for example, NP charging processes in aqueous environments. Furthermore, the charging of NPs induced by the photoemission process itself (final-state effect[25]) has to be taken into account. Finally, in the case of electrochemically prepared samples, the application of an electrostatic potential across the metal/electrolyte interface is known to result in additional binding energy shifts termed as "electrochemical shift".[26]

In this work, we present a simple alternative approach for the study of NP charging effects, which is compatible with aqueous environments and neither requires a conductive support nor UHV conditions: a field-effect capacitive electrolyte−insulator−semiconductor (EIS) device is used for the first time to trace the excess charge of supported Au-NPs induced by oxygen plasma treatment or by exposing to aqueous oxidation and reduction solutions. To verify the ability of the new approach, XPS has been used as a reference method to establish the various charge states of the NPs resulting from different sample treatments. It also provides a detailed chemical analysis of the sample surface, thereby allowing one to distinguish between binding energy shifts induced by chemical reactions with other constituents ("chemical shift"), by the photoemission process itself (final-state effect), or by the charging of NPs (the effect, we are basically interested in), respectively. Because we do not apply additional potentials during exposure of the samples to aqueous oxidation and reduction solutions or during emersion, the presence of an "electrochemical shift" can safely be excluded.

2. THEORETICAL BASIS

In previous experiments, field-effect EIS devices have been shown to be versatile tools for detecting pH, ion and analyte concentrations, enzymatic reactions, charged macromolecules (DNA, proteins, polyelectrolytes), and action potentials of living cells (see e.g., refs 27−34). In addition, it has been demonstrated that the coupling of nanoparticle/biomolecule inorganic/organic hybrids with field-effect devices could open new opportunities for biosensors and biochips.[6,7] More recently, EIS devices functionalized with Au-NPs have been used for the realization of biomolecular logic gates.[12,35] Because EIS devices are very sensitive for any kind of electrical interaction at or nearby the gate insulator/electrolyte interface, they are principally able to detect also the charge of NPs deposited onto the gate surface. Figure 1 shows a schematic of the Au-NP-modified capacitive EIS structure (in this study, Al-p-Si−SiO_2−Au-NP) which represents a (bio)chemically sensitive capacitor. Our approach is based on the idea that the flatband potential (the potential at which the energy bands in the semiconductor continue horizontally up to the surface and the net charge density in the semiconductor is zero) and capacitance of the NP-coated EIS device should reflect the potential developed on the supported bare or ligand-stabilized NPs induced by their accumulated charge. The charging of NPs will modulate the space-charge capacitance in the Si and, consequently, the capacitance−voltage ($C-V$) curve and output signal of the EIS structure. The resulting changes in the flatband potential or sensor output signal will be defined among others by the excess charge and coverage of the Au-NPs.

In general, the flatband potential of an EIS system is given by[36,37]

$$V_{fb} = \left(E_{ref} + \chi_{sol} - \frac{\Phi_s}{q} - \frac{Q_i + Q_{ss}}{C_i}\right) - \phi_0 \qquad (1)$$

where E_{ref} is the potential of the reference electrode, χ_{sol} is the surface-dipole potential of the solution, Φ_s is the work function of the electrons in the semiconductor, q is the elementary charge, Q_i and Q_{ss} are charges located in the gate oxide and the surface as well as interface states, respectively, C_i is the capacitance of the gate insulator, and ϕ_0 is the electrolyte/gate interfacial potential. In eq 1, all terms can be considered as constant except for ϕ_0, which can be a function of the pH, ion or analyte concentration, and charge of adsorbed molecules. For the EIS device covered with bare or ligand-stabilized Au-NPs, in a first approach, the term ϕ_0 can be considered as an averaged mixed potential of the insulator/solution and Au-NP/solution interface, respectively.

The total surface charge per unit area, σ, is the sum of the NPs' charge, σ_{NP}, and the acid−base charge of the SiO_2 surface not covered with Au-NPs, σ_{SiO2}

$$\begin{aligned}\sigma &= \sigma_{SiO_2}(1-f) + f\sigma_{NP} \\ &= q(1-f)([Si-OH_2^+] - [Si-O^-]) + fNQ_{NP}\end{aligned} \qquad (2)$$

where [Si−OH_2^+] and [Si−O^-] are the density of surface-protonated and deprotonated sites, N is the surface density of NPs, Q_{NP} is the excess charge per Au-NP, and the parameter f stands for the gold-coated fraction of the insulator surface. The term σ_{SiO2} is a function of the bulk pH value of the solution and of the gate material properties, such as the surface-site density and the equilibrium constants of the acid−base reactions. Because of charge neutrality, an equal, but opposite, charge is built up in the electrolyte side of the double layer. Adopting a simple double-layer capacitor model described in ref 38 (which is reasonable if the double-layer capacitance, C_{dl}, is similar at the Au-NP/electrolyte and insulator/electrolyte interface,

dx.doi.org/10.1021/jp109886s |J. Phys. Chem. C 2011, 115, 4439–4445

Scheme 1. Functionalization of an EIS Sensor with Au-NPs[a]

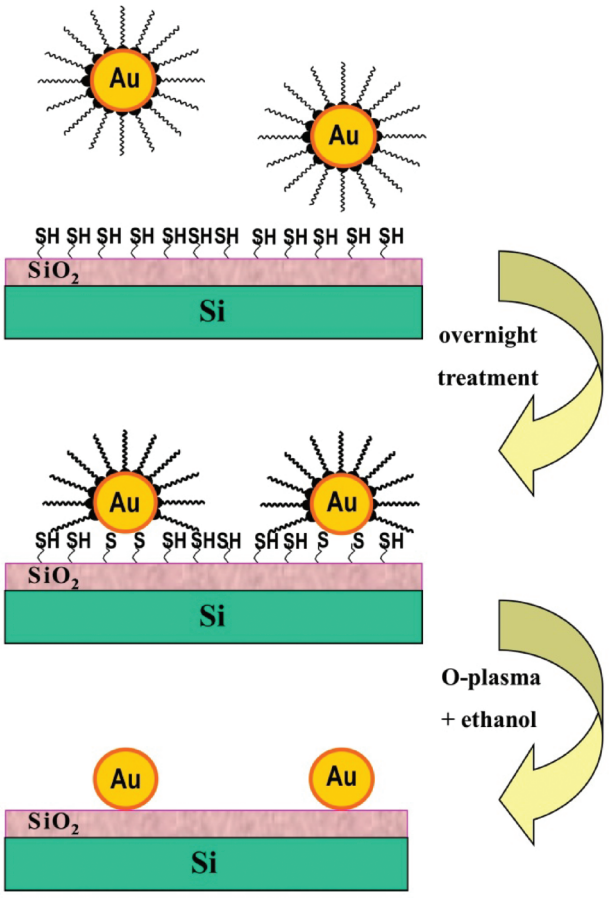

[a] Silanization of the SiO_2 surface (top), deposition of Au-NPs with organic shells from the solution (middle), and removal of organic shells by means of oxygen-plasma treatment (bottom).

respectively) and neglecting charges inside the semiconductor and insulator, the following relation between the surface potential and the total surface charge can be obtained:

$$\phi_0 = \frac{\sigma}{C_{dl}} = \frac{\sigma_{SiO_2}(1-f) + fNQ_{NP}}{C_{dl}} \qquad (3)$$

Although the above-described model represents an approximation, which does not take into account a possible screening of the NP charge by counterions in the solution, eqs 1−3 clearly illustrate that the interfacial potential and flatband potential will be affected by both the pH value of the solution (via the term σ_{SiO2}) and the excess charge of the Au-NPs. On the other hand, a measurable effect from the NPs' charge can be expected only if the term fNQ_{NP} is not significantly small compared to the charge of the insulator surface area that is not covered by NPs. Thus, a reasonably high surface coverage of NPs is required for a successful experiment. This condition is fulfilled in our experiment, as the surface coverage of NPs determined from SEM (scanning electron microscopy) micrographs was in the range of $f \approx 0.5-0.6$.

In the following, it will be demonstrated that the charge changes of Au-NPs induced by either potassium persulfate oxidation or sodium borohydride reduction or by the exposure to an oxygen plasma can easily be detected by means of $C-V$ measurements using EIS structures.

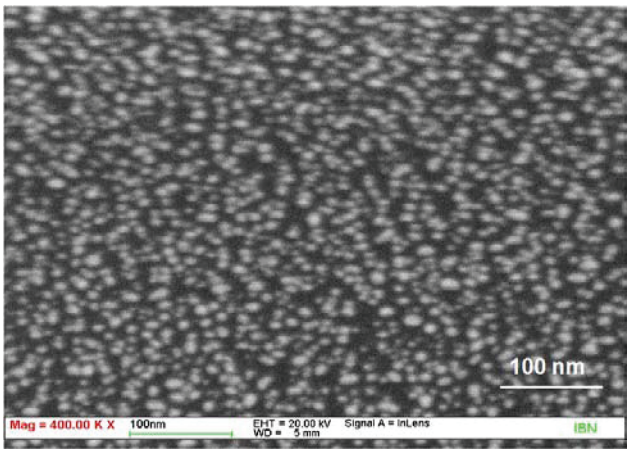

Figure 2. High-resolution SEM image of the Au-NP-coated EIS sensor surface after the removal of organic ligands using oxygen plasma.

3. EXPERIMENTAL SECTION

Sensor Preparation and Surface Modification. For the experiment, Al-p-Si−SiO_2 (thermally grown SiO_2 of 30 nm) structures with chip sizes of 10 × 10 mm^2 have been fabricated. As a contact layer, a 300 nm Al film was deposited on the rear side of the p-type Si wafer. The SiO_2 surface was cleaned and treated by oxygen plasma at 250 W for 10 s (TePLa-100E, Technics Plasma, Germany). Au-NPs of 5−8 nm in diameter were prepared according to the procedure described in refs 6 and 7 using $NaBH_4$ as a reductant for $HAuCl_4$ and tetraoctylammonium (TOA) bromide as a stabilizing capping agent for the Au-NP suspension in toluene. TOA-stabilized Au-NPs were deposited on the thiol-siloxane-modified SiO_2 surface by immersion of the sensors in toluene−gold solution for 12 h (see Scheme 1).

For silanization, the chips were exposed to a freshly prepared solution of MPTS ((3-mercaptopropyl)trimethoxysilane) in toluene (10%) at room temperature for 1 h. The thickness and homogeneity of the silane layer was controlled by imaging ellipsometry (EP3, Nanofilm, Germany). An optimal Au-NP coverage was achieved when the thickness of the silane layer was 1.6−2.0 nm, which is equivalent to the thickness of 2 ML (monolayer). To remove the organic shell (capping agent) of the Au-NPs and to simultaneously convert the thin silane layer into SiO_2, the sensors were treated with oxygen plasma of different power for 10 s, then immersed in ethanol overnight for removal of the gold oxide, which is usually formed after the oxygen-plasma treatment. As an example, Figure 2 shows a high-resolution SEM image of a Au-NP-coated EIS sensor surface. The image depicts a densely packed ensemble of gold NPs with an average density of about 1.5 × 10^4 NPs per μm^2. The density and morphology of NPs remain essentially similar after the exposure to 100 or 200 W oxygen plasma, while the treatment with 300 W plasma and higher resulted in a distinctly lower surface coverage of NPs.

XPS Analysis. Core-level spectra were acquired using monochromatized Al Kα X-rays (1486.6 eV) as provided by two commercial photoemission systems (Fisons ESCALAB 210, Physical Electronics PHI 5600LS). The binding energy scale of both instruments was calibrated by means of independent Au reference samples (Au $4f_{7/2}$: 84.0 eV). In all cases, the total energy resolution (electrons and photons) was adjusted to values between 0.30 and 0.38 eV (full width at half-maximum, fwhm).

dx.doi.org/10.1021/jp109886s |J. Phys. Chem. C 2011, 115, 4439–4445

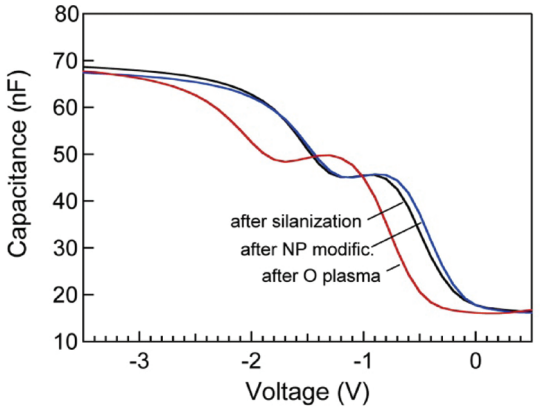

Figure 3. $C-V$ curves of an EIS structure recorded after silanization, Au-NP deposition, and oxygen-plasma treatment.

Although relatively thick gate-insulator layers (in this study, 30 nm SiO_2) are substantial for successful $C-V$ measurements in order to avoid any leakage currents, such insulating layers would result in charging of the whole sample surface during the XPS measurements. To avoid the frequently used procedure of calibrating the binding energy scale in such situations by means of carbon contaminations present at the sample surface, silicon wafers covered with native SiO_2 (layer thickness $\sim$ 1−2 nm) were taken as substrates for the XPS experiments. In this way, the Si 2p core lines of the buried Si single crystal can still be detected, enabling the precise calibration of the binding energy scale after each surface modification step.

Electrochemical Characterization. The EIS sensors were electrochemically characterized in a phosphate buffer solution of pH 7.4 by means of a $C-V$ method at a frequency of 100 Hz using an impedance analyzer (Zahner Elektrik, Germany). The $C-V$ curves were recorded after each surface modification step as well as after aqueous oxidation and reduction of Au-NPs in potassium persulfate or sodium borohydride solution, respectively. For operation, a dc polarization voltage (in the range of −3.5 to 0.5 V) was applied to the gate via a reference electrode, and a small ac voltage (20 mV) was applied to the system in order to measure the capacitance of the sensor. A Ag/AgCl electrode (Metrohm) was used as the reference electrode. The contact area of the EIS sensor with the solution was about 0.5 cm^2. The measurements were performed in a dark Faraday cage at room temperature.

4. RESULTS AND DISCUSSION

Figure 3 shows $C-V$ curves of an EIS structure recorded after the silanization, Au-NP deposition, and oxygen-plasma treatment. These curves differ from the typical $C-V$ curve of a bare EIS structure by the existence of two inflection points in the depletion range. Because this effect was first observed after the cleaning of the SiO_2 surface by the oxygen plasma before the silanization process and remains intact after the further surface-modification steps, it can be attributed to plasma-induced slow states associated with trapped positive charges in the oxide.[39] Although the $C-V$ curves are deformed, they have no impact on the basic results obtained in this work, because we are interested in shifts of the $C-V$ curves along the voltage axis in the depletion region induced by different surface modification and treatment steps. As can be seen in Figure 3, pronounced potential shifts of about 80 mV and more than −300 mV are observed in the depletion region (at ∼40 nF) after the Au-NP deposition and oxygen-plasma treatment (200 W), respectively. TOA-stabilized Au-NPs are negatively charged,[40,41] which explains the observed positive shift of the corresponding $C-V$ curve upon the Au-NPs deposition. The large shift of the $C-V$ curve (−300 mV) after the oxygen-plasma treatment in the direction to a more negative flatband potential can be attributed both to the removal of the negatively charged organic ligands and to the generation of positive charges on/close to the NPs (more likely, in a SiO_2 layer) that is supported by the subsequent XPS measurements.

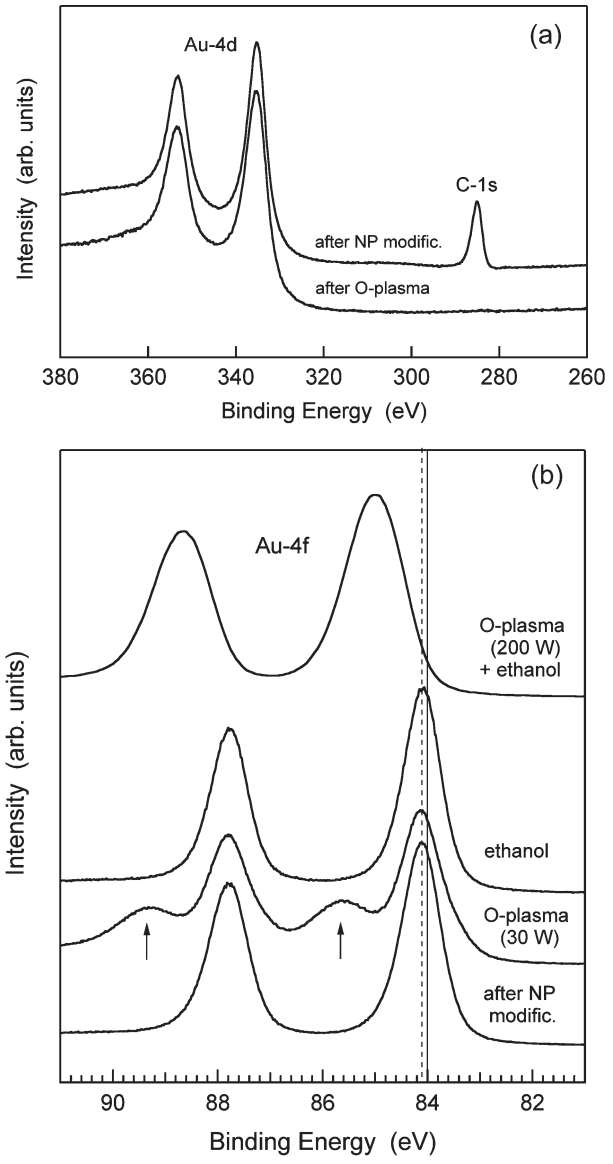

Figure 4. (a) Au 4d and C 1s core lines acquired from ligand-stabilized Au-NPs on a silanized Si−SiO_2 (native oxide) substrate before and after the in situ exposure to a weak oxygen plasma (30 W, 1 min). The oxygen plasma results in the formation of gold oxide, as inferred from the presence of an additional Au 4f component (see arrows), which, however, disappears after storing the sample in ethanol (b). In the latter case, the Au $4f_{7/2}$ position shows a shift by 80 meV to higher binding energies (dashed vertical line) as compared with a bulk Au reference sample (solid vertical line). A large binding energy shift (∼880 meV) was registered after strong oxygen plasma (200 W) treatment, followed by reduction of the corresponding gold oxide in ethanol (fourth spectrum from the bottom).

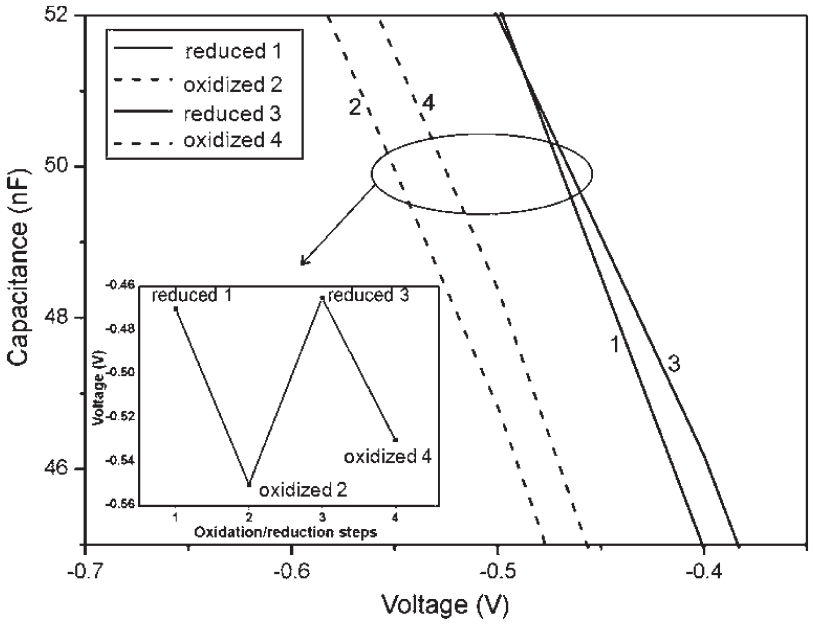

Figure 5. $C-V$ curves in the depletion region recorded after consecutively exposing a Au-NP-covered EIS structure to an oxidative (3 M potassium persulfate) or a reductive (3 M sodium borohydride) solution for 16 h. The inset graph shows the respective potential shifts evaluated at ∼60% of the maximum capacitance.

A large density ($\sim 10^{12}$ cm^{-2}) of positive charges induced in a SiO_2 layer after oxygen-plasma treatment and, as a consequence, a large negative shift of $C-V$ curves of a bare p-Si−SiO_2 structure has also been registered in ref 39.

Figure 4a presents the corresponding Au 4d core doublet together with the C 1s core line before and after the in-situ application of a weak oxygen plasma (30 W, 1 min). A vanishing C 1s intensity after oxygen-plasma treatment verifies the complete removal of the negatively charged TOA organic ligands. This is in good agreement with the $C-V$ measurements in Figure 3.

On the other hand, it is well known that the exposure of Au-NPs to oxygen plasma results in the formation of a Au oxide.[23,42] The presence of such an oxide can hardly be observed in Figure 4a due to a strong intrinsic line broadening of the Au 4d doublet. However, when the line shape of the corresponding Au 4f spectrum (Figure 4b, middle curve) is analyzed, Au oxide-induced features can easily be identified by means of a second doublet shifted by about 1.6 eV to higher binding energies ("chemical shift"). After storing the sample in ethanol overnight, this oxide-induced contribution is completely absent, reflecting now the pure elemental gold rather than a mixture of species having different oxidation states. Interestingly, after the reduction of the gold oxide contribution, a small positive shift of about 80 meV (dashed vertical line in Figure 4b) as compared to the gold reference sample (solid vertical line) can be recognized. This shift to higher binding energies (corresponding to a shift to lower kinetic energies of the photoelectrons) perfectly matches the expectation[43] for the loss of kinetic energy of a photoelectron escaping in the electrical field of a positively charged (i.e., photoionized) nanoscaled capacitor having an average diameter of 6.5 nm. Therefore, this shift can be identified as the final-state contribution induced by the photoemission process itself.[25]

On the other hand, a large binding energy shift (∼880 meV) was registered after the strong oxygen plasma (200 W) treatment, followed by the reduction of the corresponding gold oxide in ethanol (Figure 4b, fourth spectrum from the bottom). Such a large shift cannot be attributed only to charge changes in the Au-NP/shell complex caused from the removal of the organic ligands or to the positive charge remaining on the AuNPs supported on an insulating substrate during the photoemission final state. More likely, the substrate material underneath/close to the NPs might be additionally affected by oxygen plasma-generated charges trapped in the near-surface region of the SiO_2 support layer. This suggestion is supported by the observed large shift in the $C-V$ curves for a Au-NP-covered EIS structure after strong oxygen plasma treatment (see Figure 3). Moreover, because of a significant current of photoelectrons passing the surface region (nA), neutralization of these charges with time and, therefore, a backward shift of the binding energy toward its original position before plasma treatment can be expected. In fact, in our experiments, a backward shift of about −0.15 eV has been registered (not shown) 2 h after starting the X-ray source. These results as well as previously observed large differences between the binding energy shifts of Au-NPs on different insulating substrates (e.g., SiO_2, TiO_2, MgO, GaN, highly ordered pyrolytic graphite)[21,23,44−46] clearly demonstrate the important role of the substrate properties, surface/interfacial charges, and the substrate's ability to interact with the supported Au-NPs or to shield the final-state hole in the charging of the supported Au-NPs and binding energy shifts.

To validate the ability of capacitive field-effect sensors to detect the Au-NPs' charge changes induced in aqueous solutions, after the removal of the organic shells by oxygen plasma, $C-V$ curves were recorded after consecutively exposing the Au-NP-covered EIS structures to an oxidative (3 M potassium persulfate) or a reductive (3 M sodium borohydride) solution for 16 h. As an example, Figure 5 presents enlarged $C-V$ curves of a Au-NP-covered EIS sensor in the depletion region. As can be seen, storing the NP-coated sensor in a potassium persulfate solution shifts the $C-V$ curves along the voltage axis in the direction toward more negative voltages, which corresponds to

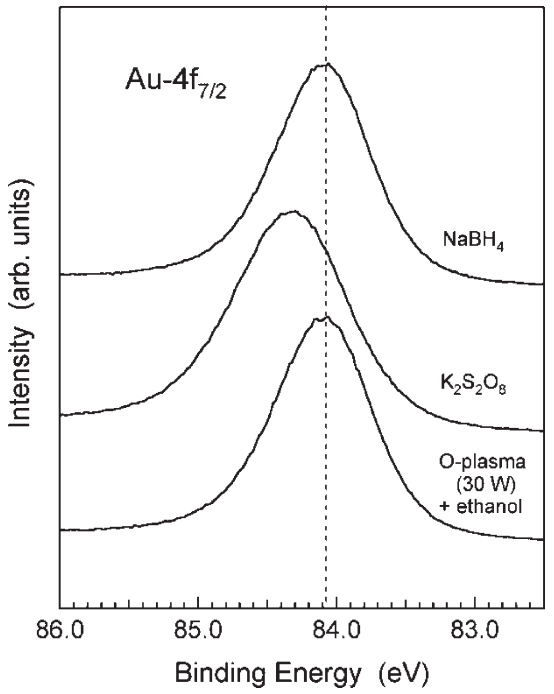

Figure 6. Au 4f spectra recorded after the exposure of the Au-NP-coated sensor surface to an oxidative (3 M potassium persulfate) and a reductive (3 M sodium borohydride) solution. Although exposing the Au-NPs to an oxidative solution results in a binding energy shift of 0.24 eV to higher values, subsequent exposure to the reductive solution turns out to fully restore its original value.

an additional positive charging of the sensor surface. On the other hand, exposing the sensor in a subsequent step to a sodium borohydride solution shifts the $C-V$ curve backward by about 80 mV. The inset graph in Figure 5 shows alternating potential shifts evaluated from the depletion region (at ~60% of the maximum capacitance) of the $C-V$ curves. The observed shifts in the $C-V$ curves can be attributed to flatband-potential changes induced by changes of the Au-NPs' charge in oxidative or reductive solutions. The charging/discharging of supported Au-NPs in aqueous solutions can be repeated in a (nearly) reversible manner, as can be also recognized in Figure 5 (inset graph).

The results of $C-V$ measurements correlate well with XPS experiments. Figure 6 represents Au 4f spectra recorded after the exposure of the Au-NP-coated sensor surface to various chemical environments, followed by carefully rinsing the samples in deionized water and drying them in a stream of nitrogen gas. Although exposing the NP-coated sensor to a 3 M potassium persulfate oxidative solution for 16 h results in a binding energy shift of 0.24 eV to higher values, its subsequent exposure for 16 h to a 3 M sodium borohydride solution turns out to fully restore its original value. It is important to note that the exposure to potassium persulfate does not result in a formation of any gold compound having a nonzero oxidation state, as can be inferred from the presence of only a single Au 4f doublet. A similar behavior is found after storing the Au-NPs in sodium borohydride solution, giving evidence for the presence of only elemental gold. To understand the shift of the Au 4f lines toward higher binding energies, the charging of NPs induced by, for example, the adsorption of a small amount of sulfate (SO_x) groups at the NPs' surface, might be assumed. This idea is, in fact, supported by

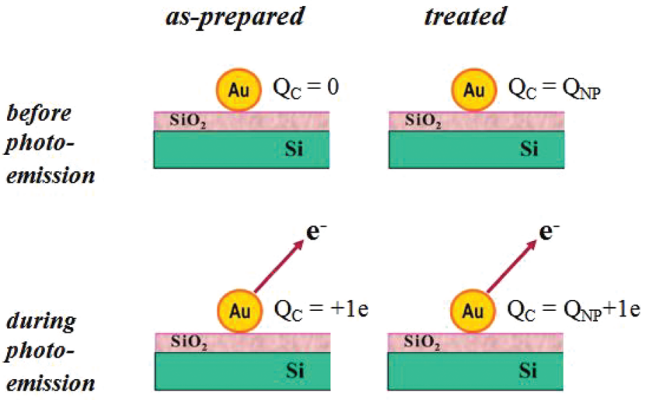

Figure 7. Scheme illustrating the final-state effect in the XPS experiment.

Table 1. Summary of Observed Au 4f Shifts, Resulting Effective Charges on NPs, and Potential Shifts in $C-V$ Curves after Different Sample Treatments

sample treatment	Au 4f shift (meV)	Au-NP effective excess charge (e)	potential shift (mV)
potassium persulfate	+240	+2	−85
sodium borohydride	−240	−2	+81
O-plasma (200 W)	+880	+10	−300

the observation of a S 2p binding energy value of 169 eV (representing S in a highly oxidized state), as detected after the storage in an oxidative solution. Sulfur, on the other hand, can no longer be observed after subsequent storing the same sample in the reductive solution, in accordance with a shift of the Au 4f doublet back toward its starting position.

To estimate the effective charge, Q_{NP}, of the Au-NPs after the different sample treatments, the XPS final-state effect measured on as-prepared nanoparticles ($Q_{NP} = 0$) can be taken as a calibration. In a simplified picture (see Figure 7), a photoelectron emitted from a neutral nanoparticle into the vacuum chamber of the electron spectrometer can be considered as escaping in the electrical field of a spherical capacitor (the nanoparticle), the latter being positively charged with exactly one elementary charge (e) corresponding to the missing photoelectron. As a result of the rather small capacitance C_{NP} of a nanoscaled capacitor, this effect will reduce the kinetic energy of the outgoing photoelectron due to Coulomb interaction by an amount proportional to e^2/C_{NP}, thus resulting in an increased binding energy value of the probed core level. In our case, a binding energy shift of 80 meV is observed for the as-prepared nanoparticles with respect to a bulk reference sample (see Figure 4b), which agrees well with expectations[43] for Au-NPs having a diameter of 5−8 nm. If additional charges Q_{NP} are stored on the nanoscaled capacitors before a subsequent photoemission experiment, the loss in kinetic energy of the outgoing photoelectrons should now scale with eQ_C/C, with $Q_C = Q_{NP} + 1e$, the latter unit charge representing again the contribution arising from the escaping photoelectron. Consequently, binding energy shifts measured after the different sample treatments allow us to extract the effective charge of Au-NPs, Q_{NP}, thereby identifying charging effects on the Au-NPs induced by their exposure to various environments.

dx.doi.org/10.1021/jp109886s |J. Phys. Chem. C 2011, 115, 4439–4445

The evaluated values for the effective excess charge of Au-NPs induced due to the exposure of the Au-NPs to various environments are summarized in Table 1 together with the observed binding energy and potential shifts (as determined from $C-V$ measurements), evidencing a clear correlation between the $C-V$ measurements and XPS results.

5. CONCLUSIONS

The obtained results demonstrate that the $C-V$ method by applying a capacitive field-effect EIS device provides a new and convenient approach to gain insight into the charge state of supported Au-NPs exposed to various environments. The ability of capacitive EIS structures to detect charge changes in bare or ligand-stabilized Au-NPs induced, for instance, by adsorption or binding/removal of molecules, redox processes, etc., could envisage a new class of (bio)chemical devices and biochips based on NP-charge-gated field-effect structures.

AUTHOR INFORMATION

Corresponding Author

*E-mail: Jennyg@Savion.huji.ac.il (J.G.), m.j.schoening@fz-juelich.de (M.J.S.). Telephone: +49 241 6009 53144. Fax: +49 241 6009 53235.

ACKNOWLEDGMENT

Financial support by the Alexander von Humboldt Foundation (J.G.), the Odysseus program of the Flemish Government, the Federal Belgium Interuniversity Attraction Poles Program VI - "Quantum effects in clusters and nanowires", and the Methusalem project "NANO" is gratefully acknowledged. The authors thank H.-P. Bochem, A. Besmehn, A. Romanyuk, and J. Baccus for technical support.

REFERENCES

(1) Zabet-Khosousi, A.; Dhirani, A. *Chem. Rev.* **2008**, *108*, 4072–4124.
(2) Daniel, M. C.; Astruc, D. *Chem. Rev.* **2004**, *104*, 293–346.
(3) Boettcher, S. W.; Strandwitz, N. C.; Schierhorn, M.; Lock, N.; Lonergan, M. C.; Stucky, G. D. *Nat. Mater.* **2007**, *6*, 592–596.
(4) Haick, H. *J. Phys. D: Appl. Phys.* **2007**, *40*, 7173–7186.
(5) Willner, I.; Baron, R.; Willner, B. *Biosens. Bioelectron.* **2007**, *22*, 1841–1852.
(6) Gun, J.; Schöning, M. J.; Abouzar, M. H.; Poghossian, A.; Katz, E. *Electroanalysis* **2008**, *20*, 1748–1753.
(7) Gun, J.; Rizkov, D.; Lev, O.; Abouzar, M. H.; Poghossian, A.; Schöning, M. J. *Microchim. Acta* **2009**, *164*, 395–404.
(8) Kim, S. K.; Cho, H.; Jeong, J.; Kwon, J. N.; Jung, Y.; Chung, B. H. *Chem. Commun.* **2010**, *46*, 3315–3317.
(9) Thibault, S.; Aubriet, H.; Arnoult, C.; Ruch, D. *Microchim. Acta* **2008**, *163*, 211–217.
(10) Ryu, S.-W.; Kim, C.-H.; Han, J.-W.; Kim, C.-J.; Jung, C.; Park, H. G.; Choi, Y.-K. *Biosens. Bioelectron.* **2010**, *25*, 2182–2185.
(11) Pita, M.; Krämer, M.; Zhou, J.; Poghossian, A.; Schöning, M. J.; Fernandez, V. M.; Katz, E. *ACS Nano* **2008**, *2*, 2160–2166.
(12) Krämer, M.; Pita, M.; Zhou, J.; Ornatska, M.; Poghossian, A.; Schöning, M. J.; Katz, E. *J. Phys. Chem. C* **2009**, *113*, 2573–2579.
(13) Kim, C. K.; Ghosh, P.; Rotello, V. M. *Nanoscale* **2009**, *1*, 61–67.
(14) Homberger, M.; Simon, U. *Philos. Trans. R. Soc., A* **2010**, *368*, 1405–1453.
(15) Lai, P. Y.; Chen, J. S. *J. Vac. Sci. Technol., A* **2008**, *26*, 1062–1067.
(16) Andres, R. P.; Bein, T.; Dorogi, M.; Feng, S.; Henderson, J. I.; Kubiak, C. P.; Mahoney, W.; Osifchin, R. G.; Reifenberger, R. *Science* **1996**, *272*, 1323–1325.
(17) Xu, L.-P.; Chen, S. W. *Chem. Phys. Lett.* **2009**, *468*, 222–226.
(18) Chen, S. W.; Templeton, A. C.; Murray, R. W. *Langmuir* **2000**, *16*, 3543–3548.
(19) Miyazaki, T.; Hasegawa, R.; Yamaguchi, H.; Ohoka, H.; Nagato, H.; Amemiya, I.; Uchikoga, S. *J. Phys. Chem. C* **2009**, *113*, 8484–8490.
(20) Lioubashevski, O.; Chegel, V. I.; Patolsky, F.; Katz, E.; Willner, I. *J. Am. Chem. Soc.* **2004**, *126*, 7133–7143.
(21) Jiang, Z.; Zhang, W.; Jin, L.; Yang, X.; Zhu, J.; Huang, W. *J. Phys. Chem. C* **2007**, *111*, 12434–12439.
(22) Tunc, I.; Korcan Demirok, U.; Suzer, S.; Correa-Duatre, M. A.; Liz-Marzan, L. M. *J. Phys. Chem. B* **2005**, *109*, 24182–24184.
(23) Lim, D. C.; Lopez-Salido, I.; Dietsche, R.; Bubek, M.; Kim, Y. D. *Chem. Phys.* **2006**, *330*, 441–448.
(24) Alvarez, M. M.; Khoury, J. T.; Schaaff, T. G.; Shafigullin, M. N.; Vezmar, I.; Whetten, R. L. *J. Phys. Chem. B* **1997**, *101*, 3706–3712.
(25) Hövel, H.; Barke, I.; Boyen, H.-G.; Ziemann, P.; Garnier, M. G.; Oelhafen, P. *Phys. Rev. B* **2004**, *70*, 0454241–0454245.
(26) Zhou, W.; Kolb, D. M. *Surf. Sci.* **2004**, *573*, 176–182.
(27) Poghossian, A.; Schultze, J. W.; Schöning, M. J. *Sens. Actuators, B* **2003**, *91*, 83–91.
(28) Mourzina, Y.; Mai, T.; Poghossian, A.; Ermolenko, Y.; Yosinobu, T.; Vlasov, Y.; Iwasaki, H.; Schöning, M. J. *Electrochim. Acta* **2003**, *48*, 3333–3339.
(29) Lee, C.-S.; Kim, S. K.; Kim, M. *Sensors* **2009**, *9*, 7111–7131.
(30) Neff, P. A.; Naji, A.; Ecker, C.; Nickel, B.; v. Klitzing, R.; Bausch, A. R. *Macromolecules* **2006**, *39*, 463–466.
(31) Poghossian, A.; Abouzar, M. H.; Amberger, F.; Mayer, D.; Han, Y.; Ingebrandt, S.; Offenhäusser, A.; Schöning, M. J. *Biosens. Bioelectron.* **2007**, *22*, 2100–2107.
(32) Siqueira, J. R., Jr.; Abouzar, M. H.; Poghossian, A.; Zucolotto, V.; Oliveira, O. N., Jr.; Schöning, M. J. *Biosens. Bioelectron.* **2009**, *25*, 497–501.
(33) Kim, A.; Ah, C. S.; Park, C. W.; Yang, J.-H.; Kim, T.; Ahn, C.-G.; Park, S. H.; Sung, G. Y. *Biosens. Bioelectron.* **2010**, *25*, 1767–1773.
(34) Poghossian, A.; Ingebrandt, S.; Offenhäusser, A.; Schöning, M. J. *Semin. Cell Dev. Biol.* **2009**, *20*, 41–48.
(35) Poghossian, A.; Krämer, M.; Abouzar, M. H.; Pita, M.; Katz, E.; Schöning, M. J. *Procedia Chemistry* **2009**, *1*, 682–685.
(36) Bergveld, P. *Sens. Actuators* **1991**, *6*, 55–65.
(37) Poghossian, A. *Sens. Actuators, B* **1997**, *44*, 551–553.
(38) van Hal, R. E. G.; Eijkel, J. C. T.; Bergveld, P. *Adv. Colloid Interface Sci.* **1996**, *69*, 31–62.
(39) Paskaleva, A.; Atanassova, E. *Solid-State Electron.* **1998**, *42*, 777–784.
(40) Wuelfing, W. P.; Green, S. J.; Pietron, J. J.; Cliffel, D. E.; Murray, R. W. *J. Am. Chem. Soc.* **2000**, *122*, 11465–11472.
(41) Song, Y.; Murray, R. W. *J. Am. Chem. Soc.* **2002**, *124*, 7096–7102.
(42) Boyen, H.-G.; Kästle, G.; Weigl, F.; Koslowski, B.; Dietrich, C.; Ziemann, P.; Spatz, J. P.; Riethmüller, S.; Hartmann, C.; Möller, M.; Schmid, G.; Garnier, M. G.; Oelhafen, P. *Science* **2002**, *297*, 1533–1536.
(43) Boyen, H. G.; Ethirajan, A.; Kästle, G.; Weigl, F.; Ziemann, P.; Schmid, G.; Garnier, M. G.; Büttner, M.; Oelhafen, P. *Phys. Rev. Lett.* **2005**, *94*, 016804.
(44) Meyer, R.; Lemire, C.; Shaikhutdinov, Sh. K.; Freund, H.-J. *Gold Bull.* **2004**, *37*, 72–124.
(45) Kim, H. K.; Jang, H. W.; Lee, J.-L. *J. Appl. Phys.* **2005**, *98*, 104309.
(46) Yang, Z.; Wu, R. *Phys. Rev. B* **2003**, *67*, 081403.